Correlation effects and excited states in conjugated polymers

G. W. Hayden and E. J. Mele
Department of Physics, University of Pennsylvania, Philadelphia, Pennsylvania 19104-6396
(Received 18 February 1986)

We apply the Hubbard-Peierls Hamiltonian to study the low-lying excited states of several model conjugated polymers. The calculations employ a numerical renormalization-group method for chains of intermediate length, and a more approximate truncated configuration-interaction scheme to extrapolate the results to longer systems. In the range of on-site Coulomb repulsion strengths of physical interest, we find that a correlated even-parity singlet excited state competes with the odd-parity singlet excitation expected in the $U=0$ limit of the model, in agreement with previous studies on the Pariser-Parr-Pople model. The lowest electronic excitations in the model are identified as triplet excitations. Self-consistently-relaxed lattice configurations surrounding these electronic excitations are studied. In addition to the stable photoexcitations predicted in the $U=0$ limit of the theory, we find that the interelectronic repulsive potential leads to a rich spectrum of competing neutral structures, which are studied and characterized. Coulomb correlations provide a mechanism for production of long-lived spin-$\frac{1}{2}$ neutral excitations for degenerate ground-state systems, and spin-1 neutral excitations for nondegenerate ground-state systems.

I. INTRODUCTION

Over the past several years there has been considerable progress in understanding the ground- and excited-state properties of simple conjugated polymers within an independent-particle theory for the valence electrons. In the most widely adopted models, the lattice Hamiltonian for $(CH)_x$ proposed by Su, Schrieffer, and Heeger (SSH) (Ref. 1) and its continuum counterpart proposed by Takayama, Lin-Liu, and Maki,[2] coupling between the π electrons and the lattice degrees of freedom is explicitly included in an appropriately parametrized form, while direct electron-electron interactions are not considered. These models predict a "dimerized" bond alternating ground state, producing a gap in the electronic excitation spectrum and interesting low-lying excitations of the system, including self-localized states in the form of solitons and polarons. An important question which is raised by this activity and which has been addressed by a number of workers is the extent to which the predictions of these "single-particle" theories may be affected by direct electron-electron interactions.[3-12] There are two aspects to this question: (a) the strength of the effective (screened) repulsive interelectron potentials in long polyenes and (b) to what extent do these affect the qualitative predictions of the noninteracting model.

In a mean-field study of the Hubbard-Peierls (HP) Hamiltonian in which a repulsive on-site interelectronic potential is added to the noninteracting Hamiltonian, the presence of a dimerized ground state has been used as a gauge of the strength of the effective repulsive terms for $(CH)_x$.[3] In the mean-field theory the on-site repulsion competes with the $2k_F$ bond order instability so that dimerization is lost above a critical repulsion strength. For parameters appropriate to $(CH)_x$ this yields $U<2t_0$ which places this polyene squarely in the "weak-" interaction limit. However, more detailed recent work has shown that the bond order instability, and hence dimerization amplitude, in the ground state need not be inconsistent with the presence of even a moderately large ($U/4t\sim 1$) repulsive potential. Using Monte Carlo,[4] valence bond,[5] variational methods,[6] and renormalization-group methods[7] a number of recent calculations have demonstrated that beyond the mean-field theory the on-site repulsion tends to enhance dimerization in the ground state into the intermediate coupling regime. Only for very large U where the relevant interactions scale is t^2/U does one recover a situation where U competes with the structural instability. Several quantitative adjustments of the effective electron-phonon coupling constants appearing in the noninteracting models and appropriate sets of on-site and nearest-neighbor off-site repulsion integrals have been subsequently suggested.[6,8]

In the context of the excited states of simple conjugated systems, the effects of the repulsion terms have also been explored extensively in a number of recent studies. In the noninteracting models, of the type discussed above, the lowest-lying electronic excitations correspond to promotion of an electron from the highest occupied to lowest unoccupied molecular orbital. This transition is dipole allowed and the transition matrix element is very large, typically ~ 2 debyes/double bond, so that the transition corresponds to an optical absorption threshold. [This picture is thought to apply to the direct absorption edge near 1.9 eV in trans $(CH)_x$.] However, careful experiments over the last 10 years have indicated that this simple and straightforward prediction of the noninteracting model is incomplete, at least for a series of finite polyenes.[13] The low-lying singlet excitations are states with the same spatial symmetry as the ground state (^1A_g in polyenes with C_{2h} symmetry), and are therefore not directly accessible by one-photon excitations. However, they are accessible in two-photon absorption measurements where they have been observed and are thought to provide a stable excited

state to which the polyene may relax nonradiatively following single-photon excitation. This result has been interpreted using the Pariser-Parr-Pople (PPP) model for the electrons, which includes electron-electron interactions with a long-range $1/r$ tail. In a series of studies on finite polyenes low-lying even-parity singlets are obtained after determinants describing two-particle excitations are included in the many-electron wave functions.[14] Although the reported theoretical work suggests that the configuration interaction is not carried to full convergence especially for the longer polyenes,[14] the variations with system size in the excitation energy to the low-lying even-parity singlets still follow those observed experimentally. One concludes that the inverted level ordering is a correlation effect and is a direct manifestation of the effects of electron repulsion in the properties of simple conjugated systems. Within the PPP model, which yields such an ordering, $U/4t \sim 1$ and $(U-V)/4t \sim \frac{1}{2}$ which would indicate that $(CH)_x$ falls into the intermediate coupling regime and indeed, in a recent study employing the HP model, the inverted level ordering in the rigid-lattice excitation spectra is obtained only for $U/4t > \frac{1}{2}$, consistent with this assignment.[7]

A weakness of the models that have been used to interpret this inverted level ordering is that until recently, the effect of lattice relaxation on these excited states has not been considered. This is understandable since even for systems with more than 10 electrons, determination of the rigid-lattice excitation spectra is a computationally demanding proposition. However, this may also be a serious shortcoming since the models which treat only the electron-lattice interaction have provided a very interesting and physically appealing picture of the lattice relaxation surrounding electronic excitations in polyenes. In the SSH model photoexcitation may be regarded as the simultaneous injection of an electron and a hole into the system, spin coupled to a singlet state. This leads to the formation and unbinding of a kink-antikink pair in the bond alternation amplitude which acts to dissociate the photocarriers. In the presence of Coulomb interactions one expects a residual confinement of the photocarriers when the $1/r$ attraction between the oppositely charged defects is balanced by the exponentially decaying repulsive elastic interkink potential. In fact even within a minimal model in which only the short-range on-site and nearest-neighbor off-site repulsion is retained, such a solitonic exciton was observed by Grabowski *et al.*[15] who explored some of its properties. Some geometry optimizations for finite polyenes with the electronic degrees of freedom described by the PPP Hamiltonian and using configuration interaction have been carried out for $N \leq 8$,[16] however, here finite system size prevents a reliable generalization to the situation for long polyenes.

Thus a number of important questions concerning the influence of electron-electron interactions on the low-lying excitations in long polyenes remains to be understood. For example, it would be important to know whether the dipole forbidden ^1A_g state persists as a low-lying excitation in long polyenes and whether it can be characterized in a simple way. Lattice relaxation is likely to affect the low-lying states and may depend on chain length as well. It would be quite interesting to learn whether the solitonic exciton picture of the relaxation accompanying photoexcitation, described by Grabowski *et al.*, is modified in any fundamental way by the presence of a moderately strong Coulomb repulsion. In addition, it would be useful to know if there are any quantitative changes if we generalize to a conjugated system with a nondegenerate ground state.

In this paper we will present results from a series of calculations we have recently completed which address these questions. The calculations we present here are of two general types. First, in order to gauge the effects of the electron-electron interactions on excited-state relaxation over a range of interaction strengths, we have carried out a series of self-consistent geometry optimizations using correlated wave functions for the Hamiltonian for the ground and excited states of a 16-site polyene. The correlated wave functions are obtained by a diagonalization of the electronic part of the HP model within a numerical renormalization-group (RG) scheme. Methods of this kind have been applied in the past to the pure Hubbard model.[17] As we show below, this scheme allows a very rapid diagonalization of the many-body Hamiltonian over a complete range of interaction strengths, at least for limited system size, and allow us to carry out the self-consistent geometry optimizations with only moderate computational effort. Using this method, we are able to investigate the effect of electron-electron interaction on the dimerization amplitude in the ground state and obtain results consistent with those recently reported using a variety of many-body techniques. We also study the effective optical gap, and the structural relaxations in the excited states, including the $2\,^1A_g$ state.

Second, in order to both interpret the numerical RG results, and to extend the study to longer systems, we have constructed a much more approximate "minimal model" which we believe includes only the essential qualitative features of the more exact calculation at $N=16$. This second approach follows the spirit of a truncated configuration interaction (CI) expansion, including only up to four-particle excitations, but involving just the four one-electron states closest to the gap. In comparison with the more exact theory at $N=16$ we find that this approximation provides a reasonable semiquantitative representation of the RG results, particularly those involving self-consistent lattice structure, though there are some quantitative deficiencies. The model studied by Grabowski *et al.* can actually be recovered as a limiting case of this reduced model, and we will identify the conditions under which this even more compact model is working well. Using our minimal model we have considered lattice relaxations accompanying various electronic excitations (including the ^1A_g states) in long systems ($60 \lesssim N \lesssim 100$), and have extended the model to study the related relaxation mechanisms in the nondegenerate system. We also study and characterize the lowest-lying triplet excitation in these models.

The general picture which emerges from this study is that for the polymers with a degenerate ground state, the presence of low-lying even-parity singlets provides only a rather minor quantitative modification of many of the

current ideas about photoexcitations in these systems based on the $U=0$ theories (with the exception of the ordering of these states). We will describe the reasons for this in more detail below, but we regard this property as a special property peculiar to the systems with degenerate ground states. In fact in our studies of nondegenerate systems, the correlation effects in the excited states are of far greater qualitative significance, and are responsible for a new kind of stable excited-state structure which is not anticipated in the $U=0$ theories. Finally we suggest a picture of the low-lying singlet excitation in these systems which makes contact both with the expected behavior of the HP model in the uncorrelated ($U=0$) limit and highly correlated ($U/4t \gg 1$) limit. The lowest-lying electronic excitations in these systems are identified as triplet excitations, and interestingly they provide an important part of the ultimate description of the low-lying singlet excitation. In the presence of perturbations which can couple to the electron spin, these triplets are likely to play an important role as metastable states which are populated indirectly following excitation into the singlet manifold.

The plan of this paper is as follows: in Sec. II we discuss the details of an RG method that we presented briefly in a previous paper.[7] In Sec. III we present results on self-consistently relaxed excited electronic states on the 16-site chain using the RG method. In addition we develop the minimal method, present tests of the method on a 16-site chain for comparison with our RG results, and use our approximate scheme to study the relaxed excited states on long chains, discussing ordering of the states, length dependence, and the nondegenerate system. Then in Sec. IV a mechanism for the decay of photoexcited states of polyacetylene is proposed based on the picture we have developed.

II. FORMALISM

We want to describe the low-lying electronic states of the HP Hamiltonian,

$$H=\sum_{i,\sigma}[t_0+\alpha(x_{i+1}-x_i)](C^{\dagger}_{i+1,\sigma}C_{i,\sigma}+\text{H.c.}) +\tfrac{1}{2}\sum_i K(x_{i+1}-x_i)^2+\tfrac{1}{2}\sum_{i,\sigma}Un_{i,\sigma}n_{i,-\sigma}\,, \quad (1)$$

where $C_{i,\sigma}$ and $C^{\dagger}_{i,\sigma}$ are the electron creation and annihilation operators for site i and spin σ, x_i are the classical ion coordinates, denoting displacements from a reference equal bond length structure, n_i is the electron number operator, and t_0, α, U, and K are, respectively, the hopping amplitude, electron-phonon coupling strength, on-site Coulomb repulsion, and effective intersite spring constant. We use $t_0=-2.5$ eV, $\alpha=8.0$ eV/Å, and $K=68.6$ eV/Å^2 throughout this paper, except where noted otherwise. Because of the presence of the Coulomb term, explicit diagonalization of the HP Hamiltonian requires a full many-body basis set. However, such basis sets grow notoriously fast with increasing system size, making direct diagonalization impractical for large systems. Methods which avoid explicit use of the basis, such as Monte Carlo methods or variational methods, are primarily useful for ground-state properties, and CI and valence bond methods,[10] which do employ explicit bases, are limited to 10 or 12 sites.

Another approach which also uses an explicit basis makes use of a scaling technique to systematically limit the basis functions retained as the system size increases. For example, an early study by Hirsch[18] used such a scaling technique to study the one-dimensional Hubbard model. The method we use, previously applied by Bray and Chui[17] to the one-dimensional Hubbard model, has more variational freedom in the basis set, permitting an accurate description of the low-lying excited states. The method works efficiently to obtain these states using the HP Hamiltonian on chains of intermediate length (~ 20 sites). Because of the additional variational freedom, the size of the basis set still increases with chain length, though not nearly as quickly as the complete basis set. Therefore, we limited our studies using this method to 16-site chains and a few 32-site calculations.

The scaling technique is illustrated schematically in Fig. 1. The chain is divided into small cells, each including a few adjacent sites, and the Hamiltonian is separated into terms with intracell electron operators and terms with intercell operators. In Fig. 1 the terms that operate within the left cell are collectively labeled H_L and those that operate within the right cell are labeled H_R. Since H_L and H_R commute they can be independently diagonalized. We choose the size of each cell to be small enough so that the size of the associated complete basis set permits efficient diagonalization with no approximations. The cell eigenvectors thus obtained are labeled ψ_L and ψ_R in Fig. 1 and are further identified by the transformation properties under operations that commute with the intracell Hamiltonian: the number of electrons N, the square of the total spin S^2, and the z component of the total spin S_z. If the left and right cells are now combined to form a larger cell with quantum numbers N_{tot}, S^2_{tot}, and $S_{z\,\text{tot}}$, the basis set of the Hamiltonian for this larger cell, labeled H_{total}, can be constructed by taking tensor products of ψ_L's and ψ_R's

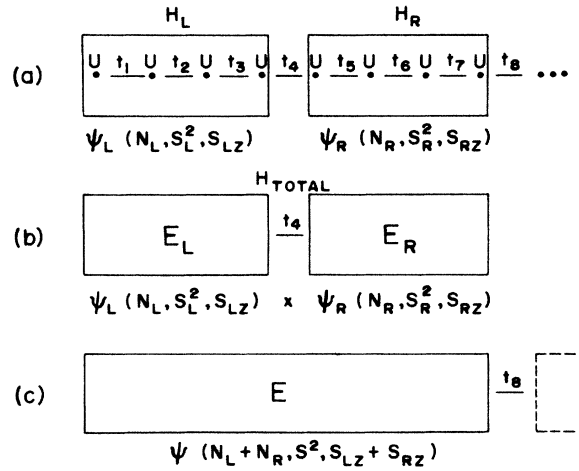

FIG. 1. Schematic presentation of the RG method. (a) Intracell Hamiltonians H_L and H_R are diagonalized yielding eigenstates ψ_L and ψ_R. (b) H_{total} is constructed for a larger cell using the product basis $\psi_L\psi_R$. (c) H_{total} is diagonalized yielding eigenvalues and eigenvectors for the larger cell, and the process is repeated.

$$\psi_{\text{basis}}(N_{\text{tot}},S^2_{\text{tot}},S_{z\,\text{tot}})=\sum_{S_{z,L}S_{z,R}} C(S_{\text{tot}},S_{z\,\text{tot}},S_L,S_{zL},S_R,S_{zR})\psi_L(N_L,S^2_L,S_{Lz})\psi_R(N_R,S^2_R,S_{Rz})\ , \tag{2}$$

where

$$C(S_{\text{tot}},S_{z\,\text{tot}},S_L,S_{zL},S_R,S_{zR})$$

is the Clebsch-Gordon coefficient coupling the left- and right-spin eigenstates to the total spin eigenstate. The diagonal elements of H_{total} are the sum of the eigenvalues E_L+E_R corresponding to the eigenvectors ψ_L and ψ_R. The off-diagonal elements include the matrix elements of the intercell terms in the Hamiltonian which is represented by t_4 in the example pictured in Fig. 1. We note that a typical off-diagonal matrix element, represented schematically as

$$\langle I_L I_R \mid C^\dagger C \mid J_L J_R \rangle\ ,$$

can be factored into

$$\langle I_L \mid C^\dagger \mid J_L \rangle \langle I_R \mid C \mid J_R \rangle\ ,$$

considerably simplifying the computation and storage requirements.

The basis set may be arranged so that the diagonal elements of H_{total} are ordered from lowest to highest. We are primarily interested in the low-lying eigenstates of this Hamiltonian. If the intercell matrix elements are small compared with the range of the diagonal elements of H_{total}, the contribution of the basis states at higher energy to the low-lying eigenstates should be small. It is then a reasonable approximation to neglect all basis states above some energy, thereby reducing the size of the otherwise unwieldly basis set.

We would like to retain about 100 basis states so that the Hamiltonian can be diagonalized in a small amount of computer time. However, several hundred to several thousand basis states may be necessary for accurate work. We therefore chose to use Lowdin perturbation theory,[19] permitting us to construct a small effective Hamiltonian improved by perhaps thousands of additional basis states. In the Lowdin scheme the full Hamiltonian, whose diagonal elements have been arranged in order of increasing energy, is divided into small "direct" space, which includes the block containing the lowest energy diagonal elements, and an "indirect" space (see Fig. 2). This division also results in two off-diagonal blocks connecting the direct and indirect spaces. An effective Hamiltonian is constructed by improving the direct space by second-order coupling through the indirect space, involving matrix elements in the two off-diagonal blocks,

$$H^{\text{eff}}_{nm}=H^{(0)}_{nm}+\sum_k \frac{H^{(0)}_{nk}H^{(0)}_{km}}{E-E_k}\ , \tag{3}$$

where k is in the indirect portion of the basis set and E is an energy chosen near the anticipated eigenvalues for which the most accuracy is required. Higher-order coupling through the indirect space is neglected. This is equivalent to setting the off-diagonal matrix elements in the indirect space equal to zero.

The smallest cells in our calculation contain 4 sites and only as many as 20 basis states, permitting exact direct diagonalization. For 8-site cells, with 1764 singlet states, we typically retained 400 states in perturbation theory in addition to the 100 states in the direct space. At the level of 16-site cells, which have about 35 million singlet states, we retained about 2000 perturbation theory states at small U/t_0, increasing by several thousand as U/t_0 increased. In the intermediate U/t_0 regime we sampled every tenth higher-lying state, weighting its contribution in perturbation theory by a factor of 10, to recover the contribution of the thousands of high-lying states. Our basis is not ideally suited to the high U/t_0 regime in which the states of interest are neutral states coupled by second-order mixing through many states in the singly ionic manifold.

Because the many-electron basis is quite complicated, information about the spatial symmetry of the wave functions and information from various correlation functions is essential for interpreting the wave functions. The 16-site chain has C_{2h} symmetry, but because the π orbitals are fixed in number and direction, reflection is the only nontrivial symmetry operation. To identify the even (A_g) or odd (B_u) states on the 16-site chain is constructed using mirror symmetric basis states, resulting in a significant savings of time and storage as well.

Correlation functions, including bond orders and spin-spin correlation functions, are calculated at each scale in a parallel construction to that of the Hamiltonian. Matrix elements O_{mn} of the operator $\hat{O}$ to be studied are tabulated between four-site basis states, ϕ_m, and stored permanently. Once four-site eigenvectors, ψ_i, have been computed, a unitary transformation of the matrix O_{mn} is performed,

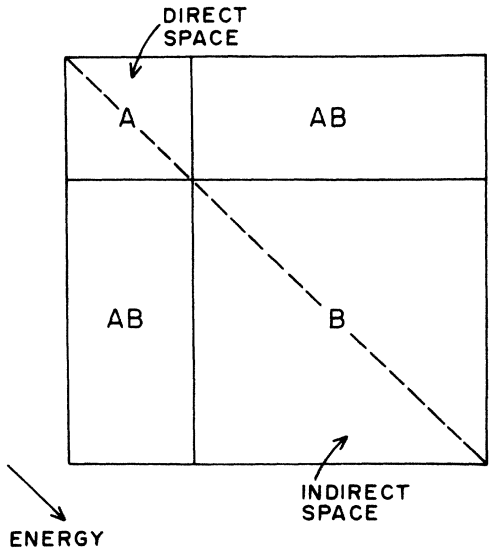

FIG. 2. In Lowdin perturbation theory the Hamiltonian is divided into "direct" and "indirect" spaces.

$$O_{ij}=\sum_{m,n} C_i^m C_j^n O_{mn} \ , \tag{4}$$

where C_i^m are the eigenvector expansion coefficients,

$$\psi_i=\sum_m C_i^m \phi_m \ . \tag{5}$$

At the next scale in the RG method matrix elements of $\hat{O}$ are constructed between basis states which are products of left and right four-site eigenvectors

$$O_{IJ}=\langle \psi_{I,L}\psi_{I,R} \mid \hat{O} \mid \psi_{J,L}\psi_{J,R} \rangle \ . \tag{6}$$

If $\hat{O}$ is an intracell operator in the left or right cell, O_{IJ} can be factored schematically as

$$O_{IJ}=\langle \psi_{I,L} \mid \hat{O} \mid \psi_{J,L} \rangle \langle \psi_{I,R} \mid \psi_{J,R} \rangle$$

or

$$O_{IJ}=\langle \psi_{I,L} \mid \psi_{J,L} \rangle \langle \psi_{I,R} \mid \hat{O} \mid \psi_{J,R} \rangle \ . \tag{7}$$

If $\hat{O}$ is an intercell operator, and can be expressed as

$$\hat{O}=\hat{O}_L \hat{O}_R \ , \tag{8}$$

then O_{IJ} can be factored schematically as

$$O_{IJ}=\langle \psi_{I,L} \mid \hat{O}_L \mid \psi_{J,L} \rangle \langle \psi_{I,R} \mid \hat{O}_R \mid \psi_{J,R} \rangle \ . \tag{9}$$

We found that it was not necessary to improve the correlation functions using Lowdin perturbation theory. However, the intercell bond orders are proportional to the intercell hopping term of the Hamiltonian, for which Lowdin perturbation theory was employed. As a result, to avoid repeating computer computations, the intercell bond orders are Lowdin improved.

Once we have calculated the bond orders we can use them in the self-consistent relaxation of the chain in the presence of an electronic eigenstate, ψ_k. Using the Hellmann-Feynman theorem, we find that the electronic force on the ith ion in the presence of ψ_k is

$$F_e^i=-\left\langle \psi_k \left| \sum_\sigma \alpha(C_{i,\sigma}^\dagger C_{i-1,\sigma}-C_{i+1,\sigma}^\dagger C_{i,\sigma})+\text{H.c.} \right| \psi_k \right\rangle \ , \tag{10}$$

where the operator whose expectation value is required is proportional to the bond orders adjacent to site i. We note that the electronic force contains no direct contribution from Coulomb repulsion terms in the case of the HP Hamiltonian since the on-site Coulomb term is x independent. We relax the chains by displacing the ions in response to the sum of the electronic and elastic forces and recomputing the electronic wave function, iterating until the net force on each site is less than 1% of the contributing forces at that site.

III. RESULTS

Now that the RG method has been presented, we would like to present the results of application of this method on a 16-site chain. We first consider the ground state of the 16-site chain, calculating the sum of the electronic and elastic energy as a function of the dimerization amplitude, $u=(-1)^n x_n$, over the range of U/t_0 shown in Fig. 3. The calculation was performed in the presence of forces $(8\alpha/\pi)$ at the ends of the chain which are required to prevent the chain from collapsing under relaxation. In Fig. 3 we have plotted the dimensionless dimerization amplitude $\delta=(\alpha u/t_0)$ at the total energy minimum against U/t_0 for three values of the dimensionless electron-phonon coupling constant $\lambda=(2\alpha)^2/\pi t_0 K$. We observe that the equilibrium dimerization amplitude is enhanced as U/t_0 is increased, with a maximum occurring at $U/4t_0=1$, the canonical crossover between the Peierls regime at small U/t_0 and the spin-Peierls regime at high U/t_0. Dimerization enhancement has been previously reported in several calculations using different methods,[4–6] and the decrease in enhancement with increasing λ, apparent in Fig. 3, has also been discussed.[6] Dixit and Mazumdar[20] have described the reason for the enhancement in the context of valence bond theory. With increasing U/t_0 valence bond diagrams that lead to dimerized configurations contribute more to the wave function, as diagrams with ionic configurations are pushed to higher energy. At high enough U/t_0, however, hopping is blocked, reducing the bond orders and the dimerization. The enhancement may also be viewed as the result of cooperation between the bond order wave and spin-density wave, which drive the dimerization at small and large U/t_0, respectively. In Fig. 4 we have plotted the ground-state bond orders and nearest-neighbor spin-spin correlation functions, $4\langle S_{zi}S_{zi+1}\rangle$, at $U=0$ and $U/t_0=4$. The calculation is presented for ground-state geometries and fixed chain ends. We note that the bond orders decrease with increasing U/t_0 and the spin-spin correlations increase on the odd bonds as U/t_0 increases. Both the bond orders and spin-spin correlations are strongest across the double bonds, so that they cooperate to enhance the dimerization amplitude.

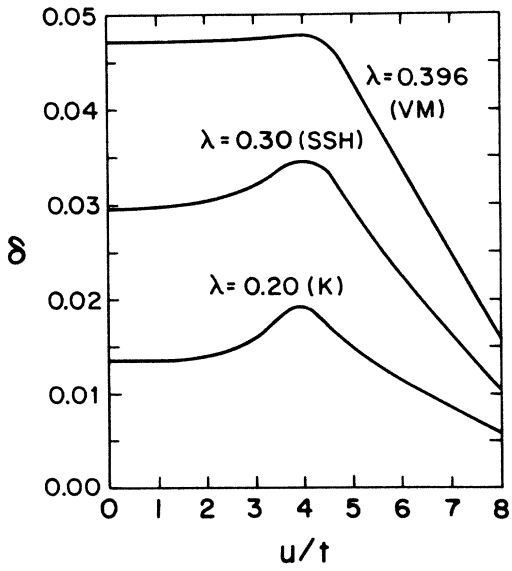

FIG. 3. Dimensionless dimerization amplitude versus strength of on-site Coulomb term for three values of dimensionless electron-phonon coupling constant on a 16-site chain.

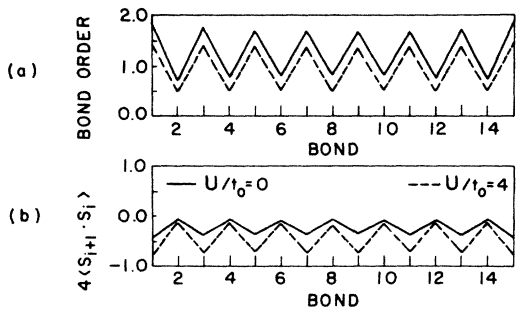

FIG. 4. (a) Bond orders for bond i, $\sum_{k,\sigma}\langle\psi_k|C^\dagger_{i,\sigma}C_{i+1,\sigma}+C^\dagger_{i+1,\sigma}C_{i,\sigma}|\psi_k\rangle$, where k is summed over filled states, and (b) nearest-neighbor spin-spin correlation functions for each bond of a 16-site chain at $U=0$ and $U/t_0=4$.

The RG method also provides heretofore inaccessible information about the low-lying excited states, so we have investigated the rigid-lattice excitation spectrum for the ground-state equilibrium dimerization configuration for various values of the repulsion strength U/t_0. In Fig. 5 we have plotted the energies of the two lowest-lying singlet excited states relative to the ground state as a function of U/t_0. The ^1B_u state at $U=0$ corresponds to excitation across the gap in the one-electron spectrum. This state is dipole allowed at $U=0$, and though our method does not determine the electron-hole symmetry of the states, the ^1B_u state at high U is known to have the same electron-hole symmetry as the ground state and is therefore not dipole allowed. We have indicated the likely crossover point of the two ^1B_u states in Fig. 5. We note that the two states cross at $U/t_0=2$, so that the dipole forbidden ^1A_g state is the lowest excited state for intermediate values of U/t_0. Dixit and Mazumdar[20] have pointed out that the ^1A_g wave function contains more covalent (neutral) valence bond diagram contributions, while the ^1B_u state contains more ionic contributions, so that the ^1A_g state must become lower than the ^1B_u as U is increased. Since the ^1A_g state is observed to be lower than the ^1B_u state in short polyenes,[13] we expect the appropriate physical value of U in the HP Hamiltonian to be in the intermediate regime, with $U/t_0\sim 2$ to 4. We observe in Fig. 5 that in this regime the Coulomb contribution to the optical gap is quite significant, amounting to 40% of the calculated gap. However, the gap is not dominated by the Coulomb contribution as has been suggested by a recent Monte Carlo study which follows the decay of the current-current correlation function in imaginary time for $\lambda=0.29$.[4]

The rigid-lattice spectrum leaves out the effects of lattice relaxation on the excited electronic states, so we now turn to a discussion of the low-lying excited states in their relaxed lattice configurations. We obtained the relaxed configurations for the system excited into a particular electronic state by displacing the sites in response to the sum of the net force, where the electronic contribution is proportional to the bond orders. We iterated the calculation of the eigenstates and forces until the net force on each site became less than 1% of the contributing forces. Relaxations were performed with the chain ends fixed in place. In Figs. 6 and 7 we show the relaxed lattice configurations in the low-lying singlet states at $U=0$ and $U/t_0=2$. For bond n we have plotted the alternating bond-length change $(-1)^n(x_{n+1}-x_n)$. Next to the $U=0$ configurations the occupation of four one-electron levels near the gap are shown. The first and second excited states are generated by one- and two-particle excitation across the gap, respectively, and both form two-soliton relaxed states. The third excited state, a two-polaron state, results from a single-particle excitation from below the band edge across the gap. We note that in the cases of the ^1B_u and $2\,^1A_g$ states, two electrons are associated with defect levels, while four electrons are associated with defect

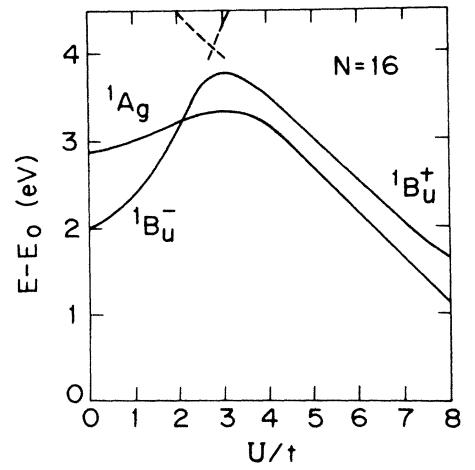

FIG. 5. Energy of first two excited states relative to the ground state as a function of the strength of an on-site Coulomb term on a 16-site chain. Inferred state crossing is indicated by dashed lines.

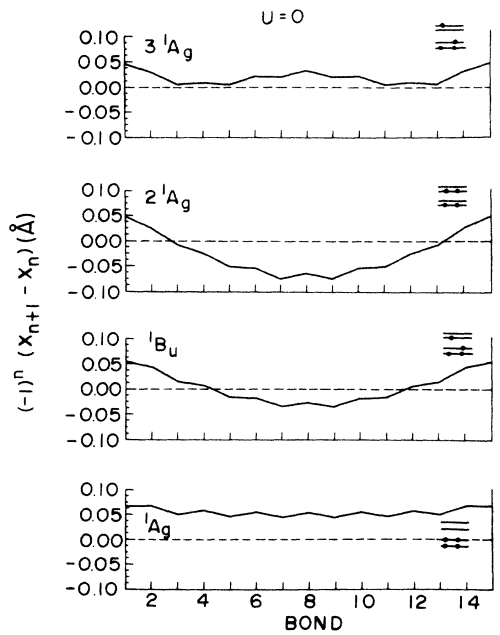

FIG. 6. Relaxed lattice configuration in first four electronic states at $U=0$ on a 16-site chain. Schematic one-electron level diagrams are adjacent to each configuration.

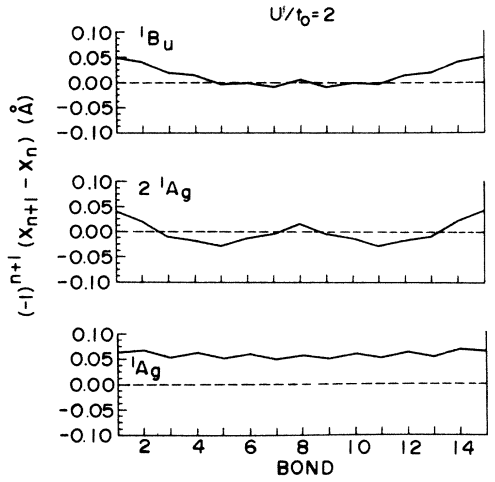

FIG. 7. Relaxed lattice configuration in first three electronic states at $U/t_0=2$ on a 16-site chain.

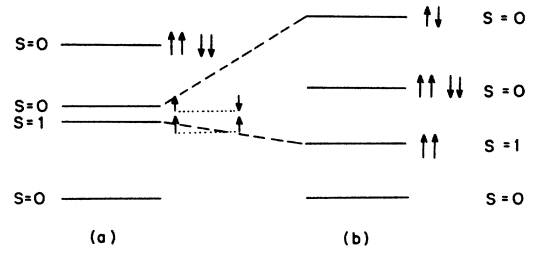

FIG. 8. Level diagrams for (a) weak coupling of neutral spin-$\frac{1}{2}$ solitons, (b) strong coupling of neutral spin-$\frac{1}{2}$ solitons. Arrows indicate spins of the unpaired electrons associated with the solitons.

levels in the $3\,^1A_g$ state. As $U/t_0=2$, the relaxed ^1B_u state closely resembles the ^1B_u at $U=0$, but with some binding of the soliton pair. However, the $2\,^1A_g$ state at $U/t_0=2$ resembles the $3\,^1A_g$ state at $U=0$ rather than the $2\,^1A_g$ state.

Further insight can be gained by considering the lowest excited states at high U/t_0. In this limit the low-lying excited states result from spin flips relative to the antiferromagnetic ground state. For Heisenberg spins coupled to the lattice degrees of freedom one spin flip produces the lowest excited state, a ^3B_u state with the triplet coupled spins associated with repelling solitons on the spin-Peierls structure.[21] The ^3B_u state is also the lowest excited state at smaller U/t_0. In this case it is favored over the ^1B_u state due to Hund's rule. If the two solitons are far apart, the singlet and triplet constructed from two weakly interacting neutral spin-$\frac{1}{2}$ excitation are nearly degenerate, so that we would expect the next highest state to be a two-soliton singlet state. However, on the 16-site chain there is a significant overlap of the electronic wave functions associated with the solitons, and this will split the triplet and singlet two-soliton states, as shown in Fig. 8. In the limit in which the spatial overlap is large, the lowest excited singlet state can be constructed by flipping two spins to produce a pair of triplets which can be coupled to form a "four-soliton" ^1A_g state at nearly twice the excitation energy of the ^3B_u state. In fact, for short chains, using the PPP Hamiltonian, Schulten *et al.*[14] find that the excitation energy of the $2\,^1A_g$ state is roughly twice that of the ^3B_u state. To see whether we can interpret the $2\,^1A_g$ state at $U/t_0=2$ as such a pair of ^3B_u two-soliton states, we relaxed the lowest state of the eight-site chain in the triplet manifold with fixed chain ends each at $U/t_0=2$. In Fig. 9 we plot two such relaxed ^3B_u states side by side and compare them with the 16-site $2\,^1A_g$ state relaxed at $U/t_0=4$. There is a strong resemblance of the two ^3B_u's and the $2\,^1A_g$. Furthermore, since the 16-site chain is constructed by connecting two 8-site chains, eigenvectors can be decomposed into a sum of products of left and right 8-site eigenvectors. When we perform this decomposition on the $2\,^1A_g$ state we find a significant amplitude for triplets on the left and right chain halves. The fact that the center two lattice defects form a polaron instead of two solitons is probably associated with singlet coupling of the two spins involved, though it is difficult to examine this using the left-right decomposition that we have made.

Because the correlation length associated with the defect states is about 15 lattice sites at small U/t_0, lattice defects associated with the relaxed ^1B_u and $2\,^1A_g$ states at $U/t_0=2$ are clearly confined on a 16-site chain. To study states with unconfined lattice defects requires a chain of at least 60 sites, which in practice is beyond the present capabilities of the numerical RG method employed. The limitation on the application of the RG method to longer chains is the size of the correlated basis set. The large basis set is necessary for accurate quantitative work, but it is conceivable that only a few degrees of freedom would suffice for determining the qualitative features of the longer correlated chains. For example, near $U=0$ we might expect that only one- or two-particle excitations to states near the lower edge of the conduction band would be important to the low-lying part of the correlated spectrum. If we consider the case of the one-electron spectrum associated with a two-soliton configuration on a long chain at $U=0$, contrasted in Fig. 10 with the spec-

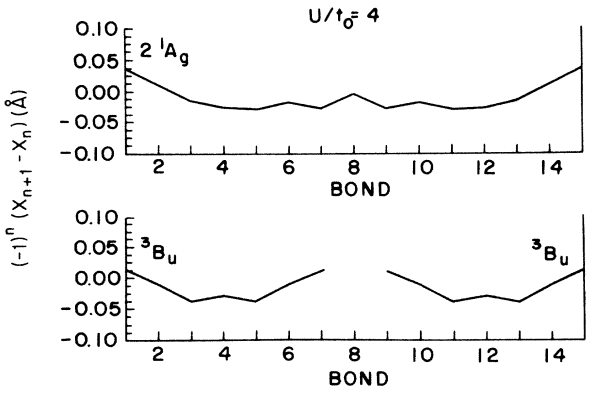

FIG. 9. Comparison of relaxed lattice configurations at $U/t_0=4$. Top: $2\,^1A_g$ state on 16-site chain. Bottom: two ^3B_u states on 8-site chains.

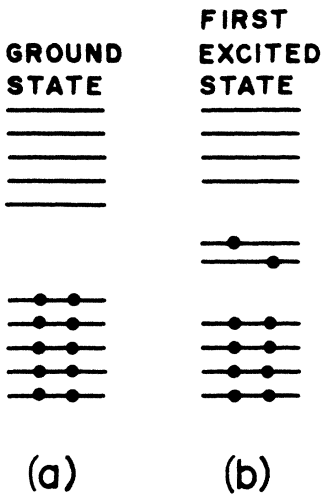

FIG. 10. Schematic one-electron level diagrams in (a) ground state and (b) two-soliton (^1B_u) states.

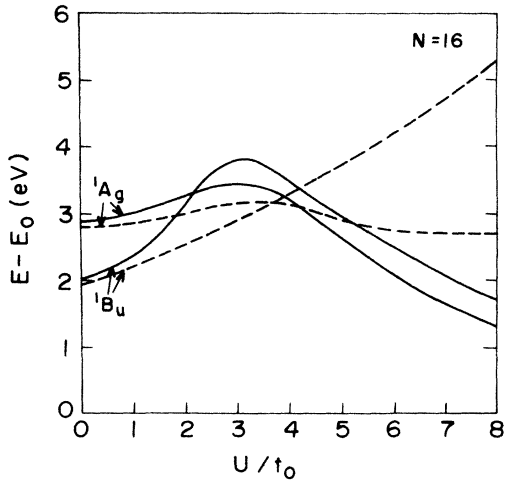

FIG. 11. Comparison of first two excited states relative to the ground state as a function of U/t_0 on a 16-site chain using the RG method (solid curves) and the reduced CI method (dashed curves).

trum in the ground-state geometry, we note that since the two defect levels are well separated from the band edges, the dominant correlation effects should result from excitations within the defect levels. Grabowski *et al.*[15] in fact have used such a model involving only correlation of the electrons in deep defect levels. Since we have found that a 4-defect state appears among the low-lying excitations on the 16-site chain, we have constructed an expanded approximate model in which 4 one-electron states are correlated. The remainder of the uncorrelated one-electron states are allowed to contribute to the bond orders, used in the relaxation of the chain.

To see whether the approximation produces reasonable results and to gain some understanding of when it breaks down, we can compare calculations on the 16-site chain to results using the RG method. We expect the minimal scheme to work best at small U/t_0, since it is based initially on a one-electron picture, and to break down completely at high U/t_0, where excitations to higher one-electron levels and excitations involving more than four electrons are likely to be important. We have calculated the total energy as a function of the dimerization amplitude at increasing U/t_0 and find that in contrast to the RG method results there is little enhancement of the equilibrium ground-state dimerization amplitude as U/t_0 is increased from zero, and that the dimerization amplitude drops off more rapidly than in the fully correlated case. This is because there is insufficient spin-wave character, due to the reduced amount of correlation, to reinforce the decreasing bond orders at higher U/t_0. We have also calculated the rigid-lattice excitation spectrum at the equilibrium dimerization using the minimal method, and in Fig. 11 we compare the rigid-lattice excitation spectrum in the ground-state geometry on the 16-site chain calculated using the minimal method and the RG method. The agreement is quite good at small U/t_0 and the spectrum obtained from the reduced CI method shows the crossing of the ^1B_u and $2\,^1A_g$ states, though at a higher value of U/t_0 than in the spectrum obtained using the RG method. It is clear that the ^1B_u state is poorly described in the high U/t_0 regime, where the approximation in the minimal method is expected to break down even though the $2\,^1A_g$ state is qualitatively correct. Since we are particularly interested in relaxed geometries, we compare in Fig. 12 the relaxed $2\,^1A_g$ state at $U/t_0=4$ using both methods. The agreement between the relaxed $2\,^1A_g$ configurations using both methods is quite good. Even though eigenvalues at $U/t_0=4$ are not quantitatively reproduced, the ordering of the low-lying states and the lattice configurations at $U/t_0=4$ recovered by the minimal method are in good agreement with the results of the RG method.

Having found that the minimal model produces good quantitative results at small U/t_0 and qualitative results at intermediate U/t_0, we now apply the model to long chains inaccessible to the RG method. We displace the sites in response to the sum of the electronic and elastic forces, recomputing the eigenstates and iterating until the net forces on the lattice sites become small. We first consider the results of relaxing the ^1B_u and ^3B_u excited states. Since the basis states in the minimal method consist of various excitations across the gap in the one-electron spectrum, we can relate the wave functions at $U\neq 0$ to one-particle excited states at $U=0$. For all values of $U\neq 0$, the ^1B_u and ^3B_u wave functions contain predominantly the one-particle excitation present at $U=0$. In Figs. 13

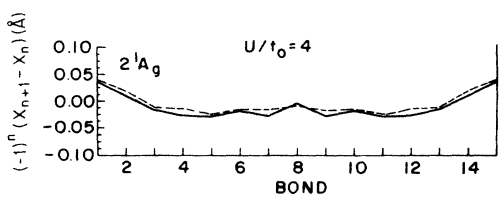

FIG. 12. Comparison of the relaxed $2\,^1A_g$ lattice configuration at $U/t_0=4$ on a 16-site chain using the RG method and the reduced CI method.

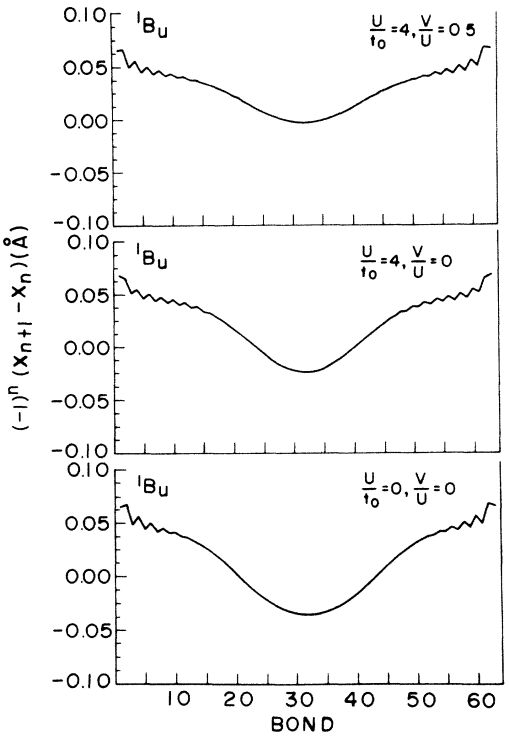

FIG. 13. Soliton binding in the ^1B_u state. Top: $U/t_0=4$, $V/U=0.5$. Middle: $U/t_0=4$, $V/U=0$. Bottom: $U=0$, $V=0$.

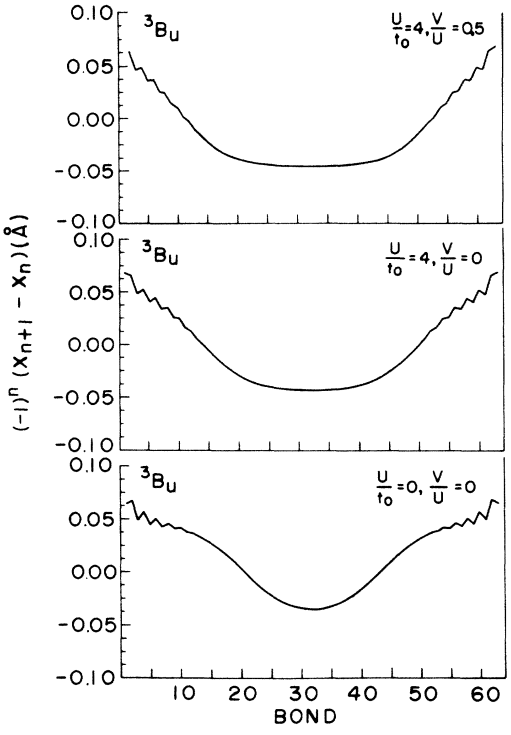

FIG. 14. Soliton repulsion in the ^3B_u state. Top: $U/t_0=4$, $V/U=0.5$. Middle: $U/t_0=4$, $V/U=0$. Bottom: $U=0$, $V=0$.

and 14 we show the relaxed ^1B_u and ^3B_u states at $U=0$, $U/t_0=4$, and at $U/t_0=4$ with $V=\frac{1}{2}U$, where V is a nearest-neighbor Coulomb repulsion added to the HP Hamiltonian. Because the charge densities associated with the two B_u solitons at $U=0$ sit on alternate sublattices we might expect there to be no interaction of the two solitons if only an on-site Coulomb repulsion term is present in the Hamiltonian. However, when a nearest-neighbor repulsion term is included, then the solitons, which carry opposite charges, would be expected to attract forming a bound exciton. We see in Fig. 13 by comparing to the $U=0$ configuration, that the ^1B_u state forms a bound excitation in the presence of V, but that binding also occurs at $U/t_0=4$ without V. If we correlate only two electrons instead of four in the minimal scheme, we indeed find no binding of the solitons for $V=0$, in agreement with results of Grabowski *et al.*[15] However, the increased correlation involving band states results in an indirect interaction between the solitons with only an on-site Coulomb repulsion. Similarly, we observe in Fig. 14 that the two solitons with aligned spins in the ^3B_u state repel for $V=0$ and $U\neq 0$ if four electrons are correlated even though only two of the electrons are directly associated with the lattice defects.

In Fig. 15 we compare at $U/t_0=4$ the ^1B_u and ^1A_g states both of which contain two solitons on the 64-site chain. We see that binding is not apparent in the ^1A_g state. This is because the ^1A_g state has little charge transfer character, while the ^1B_u state contains charged solitons.

In Fig. 16(a) we compare the $2\,^1A_g$ states on the 16- and 64-site chains at $U/t_0=4$. The 16-site state resembles more closely the $3\,^1A_g$ state at $U=0$, while the 64-site state resembles the $2\,^1A_g$ state at $U=0$. The latter state at $U=0$ results from exciting two electrons across the gap, while the former state at $U=0$ results from a one-electron excitation shown in the level diagram in Fig. 16(b). On the long chain the one-electron defect levels in the gap, associated with two solitons, are close together and well separated from the band states. The dominant correlation effects at small U should mainly involve excitations

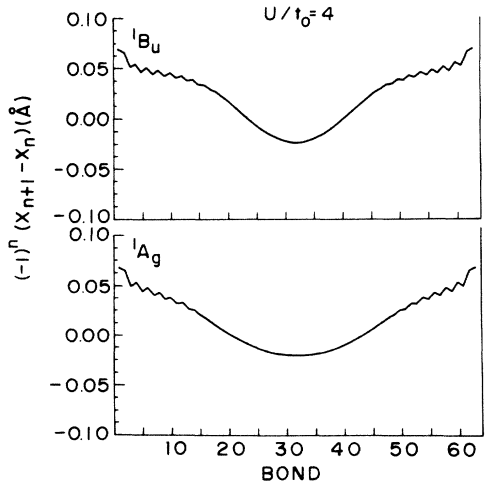

FIG. 15. Comparison of ^1B_u and ^1A_g two-soliton states at $U/t_0=4$ on 64-site chain.

among the two-defect levels, and the $2\,^1A_g$ state should thus be a two-defect state associated with two-particle excitation from the lowest to upper defect levels, in agreement with the prediction of Grabowski *et al.* On the short chain, however, the defects are confined and the electronic defect states are strongly split in energy. Correlations involving excitation into the band states become more important, and the lowest such excitation in this configuration is a one-particle excitation from the lower defect level into the conduction band resulting in a four-defect state (which is not included in the model of Grabowski *et al*). If $2\Delta_0$ is the gap and $2\omega_0$ is the separation between the defect levels, then the two-particle excitation between defect levels will have lower energy than the one-particle excitation to the conduction band if

$$4\omega_0 < \Delta_0 + \omega_0 \,. \tag{11}$$

In Table I we check this criterion for the 16- and 64-site configurations shown in Fig. 16 and see that though the 64-site structure is correctly predicted, the 16-site structure is incorrectly predicted. This is simply because we

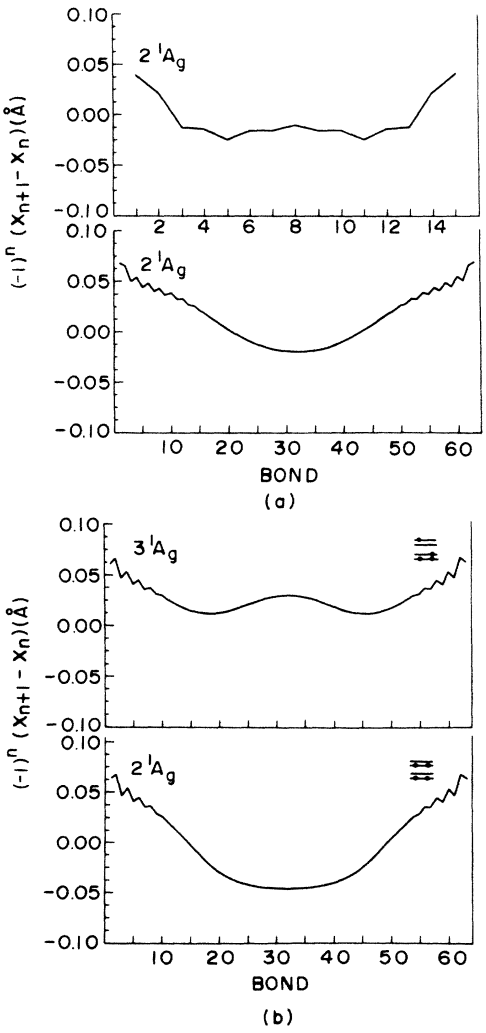

FIG. 16. Comparison of (a) $2\,^1A_g$ states on short (16-site) and long (64-site) chains to (b) ^1A_g states at $U=0$ on 64-site chain.

TABLE I. Number of defects predicted using energy-level criterion.

	$4\omega_0$	$\Delta_0+\omega_0$	Number of defects
16 site	1.79 eV	2.18 eV	2
64 site	0.52 eV	0.85 eV	2

are not in the small U/t_0 regime and several one- and two-particle excitations have significant weight in the reduced CI calculation.

We can also compare the $2\,^1A_g$ states on the short and long chains shown in Fig. 16(a) from the high U/t_0 point of view in which spin excitations provide the appropriate picture. As mentioned above, the first relaxed excited state in this picture contains triplet coupled solitons. For the first excited singlet state there is a competition between two possibilities, shown in Fig. 8. At about twice the excitation energy for the ^3B_u soliton pair we might expect a $2\,^1A_g$ four-soliton state which can be thought of as a pair of ^3B_u soliton pairs coupled to singlet. There should also be a ^1A_g state consisting of a singlet coupled pair of neutral solitons. The precise level order depends on whether it costs less energy to flip one of the triplet spins to form a two-soliton singlet state, or to generate a second triplet excitation, then coupling the two triplets to a singlet. On a long chain, the two solitons overlap weakly and therefore an exponentially small energy change should result from flipping the spin of the electron localized on one of the solitons. Therefore the $2\,^1A_g$ state should be characterized as a two-soliton neutral state on the long chain. On a short chain, however, the soliton electronic wave functions overlap strongly, splitting the triplet and singlet coupled soliton pair states. The singlet two-soliton state would then be expected to be pushed higher than the four soliton $2\,^1A_g$. At intermediate values of U/t_0 the two singlet excitations are quantum mechanically mixed. Thus we see a tendency to form a four-soliton $2\,^1A_g$ state on the 16-site chain at intermediate U/t_0 (Fig. 9), but the center two defects are not well-formed solitons. On very short chains we should also note that there may be too few spins for either of these limits to provide an adequate description of the excitation.

There is another class of systems, polymers with a nondegenerate ground state, for which intrinsic confinement rather than system size plays a central role in the structure of defects in the dimerized lattice configuration. The HP Hamiltonian as written in Eq. (1) has a degenerate ground state for an extended chain. However, to describe the class of systems with a nondegenerate ground state we can add a confinement term

$$H_c = \sum_n (-1)^n t_c \tag{12}$$

which enhances the strengths of the "odd" bonds and weakens the "even" bonds, breaking the ground-state degeneracy. The effect of H_c on the structural defects is to confine them, thus reducing the length of chain between the defects which has the higher energy configuration. The confinement of two solitons also affects the one-

electron energy levels in the gap at $U=0$. The one-electron levels for this case are shown in Fig. 17(a) and the same levels for the degenerate system are shown for comparison in Fig. 17(b). Instead of defect levels at the center of the gap in the degenerate case, there are now two shallow defect levels, split by mixing due to the confinement of the solitons. The degree of confinement is given by the confinement parameter[22]

$$\gamma=\frac{\Delta_e}{\lambda\Delta_0}\ , \tag{13}$$

where λ is the dimensionless electron-phonon coupling constant, Δ_0 is one-half the gap, and $\Delta_e=2t_c$. In our discussion of the $2\,^1A_g$ state confined in a short chain we found that

$$4\omega_0 \gtrless \Delta_0+\omega_0$$

characterized the crossover from the regime in which a two- or four-defect lowest-lying ^1A_g state occurred. Following Onodera's results[23] we find that this can be connected to a condition on the confinement parameter

$$\gamma>\gamma_c\ , \tag{14}$$

where $\gamma_c=0.68$ for the case of the $2\,^1A_g$ state. It has been suggested that cis-polyacetylene corresponds to $\gamma=0.6$, roughly equal to γ_c. We therefore expect that the relaxed $2\,^1A_g$ state in cis-polyacetylene should be characterized by four interacting defects. We relaxed a 64-site chain in this electronic state at $U/t_0=4$ using our reduced CI method and show the equilibrium lattice configuration in Fig. 18. The other ^1B_u and ^3B_u states at $U/t_0=4$ and for $\gamma=0.6$ are included for completeness. We see that indeed there are four defects in the $2\,^1A_g$ lattice configuration for $\gamma=0.6$. From the high U/t_0 point of view, the soliton electronic wave functions strongly overlap pushing the singlet polaron (bound two-soliton) singlet state above the singlet two-polaron state that we observe.

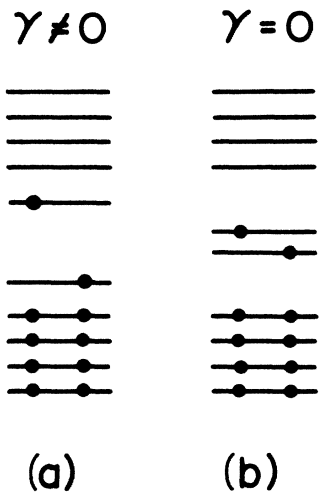

FIG. 17. Schematic one-electron level diagram on two-soliton state in the (a) nondegenerate case and (b) degenerate case.

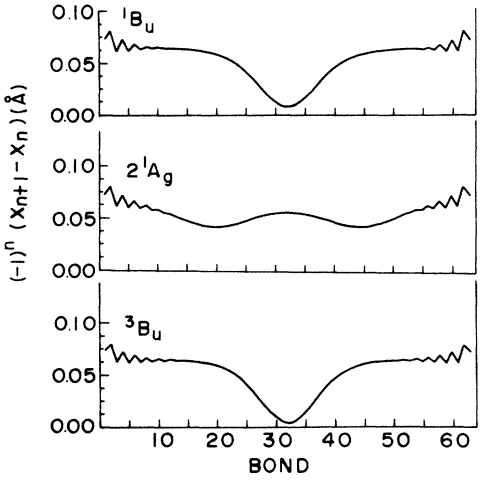

FIG. 18. First three relaxed excited states at $U/t_0=4$ on a nondegenerate 64-site chain with $\gamma=0.6$.

IV. DISCUSSION

In this section we will summarize the results of the calculations in Sec. III, the relation to some previous theoretical work and discuss some of the experimental implications of these calculations.

The experimental evidence favoring the presence of an ^1A_g state as the lowest-lying singlet excitation for finite polyenes has been summarized in several recent reviews.[13,24] From the data presented in Fig. 5, within the Hubbard-Peierls model, this ordering would require an on-site repulsion strength $U/4t_0>0.5$, which suggests that $(CH)_x$ is in the intermediate coupling regime where interaction effects and band effects are of comparable significance. Since the HP Hamiltonian explicitly treats only the short-range part of the interelectronic potential, we would expect this assignment to persist into the long-chain limit.

How can we characterize the low-lying electronic excitations in this regime? There are two kinds of important singlet excitations. The first of these is familiar from the numerous studies of the noninteracting ($U=0$) version of this model, and corresponds to the promotion of an electron from the highest occupied molecular orbital to the lowest unoccupied one-electron state. This transition is strongly dipole allowed and creates the ^1B_u excitation of the system. We find that in the presence of moderately strong electron-electron interactions, the lattice relaxation effects in this state are extremely similar to those previously studied in the $U=0$ SSH model, namely, the ^1B_u excitation spontaneously decays into a pair of oppositely charged kinks (see Figs. 6 and 7). An important difference is that the presence of U only provides a residual excitonic binding of this pair. This effect was not observed in the previous studies of Grabowski *et al.*, who did observe such an excitonic confinement only when the nearest-neighbor repulsion term, V, was turned on. In our calculations we have found that the presence of V certainly enhances the binding, but that the mixing of higher-lying one-particle excitations into the ^1B_u wave function

(not included in the calculations of Ref. 15) in the presence of U only provides an indirect interaction which tends to bind the oppositely charged pair. Aside from this relatively weak effect, the general picture from the $U=0$ SSH model of photoexcitation to oppositely charged kinks appears to survive into the intermediate coupling regime.

The second type of singlet excitation is an even-parity excitation and is somewhat more interesting since it reflects more directly the presence of interaction effects in the excited-state spectrum. For intermediate U the $2\,^1A_g$ state is the lowest-lying singlet excitation (as noted above). From our $N=16$ studies we see that the lattice relaxation surrounding this excitation is qualitatively different from that in the ^1B_u state. We identify a limit in which the *relaxed* $2\,^1A_g$ as a complex of *four* interacting defects; decomposition of the many-particle wave function shows that this excitation can be interpreted as a bound pair of triplet excitation, each of which is expected to yield a neutral kink-antikink pair in the $U=0$ limit. We interpret the equilibrium structure shown in Fig. 9 as a complex consisting of the resulting four bound neutral excitations. It is favored energetically over the ^1B_u excitation because of the larger charge transfer character in the latter odd-parity singlet state. In Fig. 16 we compared this short-chain $2\,^1A_g$ configuration to that on a long chain, were we found two defects instead of four. We can interpret the short- and long-chain results at intermediate U/t_0 in terms of pictures at both the low- and high-U/t_0 limits. First we consider many-electron configurations in the one-electron levels. On the long chain, the defect levels associated with two well-separated solitons are near the center of the gap, so that the most important excitations should be within the defect levels. For this reason we believe that even though the calculation of Grabowski *et al.* did not focus on the $2\,^1A_g$ state, their model, which correlates only the defect levels, is a quite reasonable scheme for the description of the low-lying excited states of extended polymers with a degenerate ground state. However, in the short-chain case, the defect levels are strongly split by the interaction of the wave functions associated with the defects, so that excitations into the band become significant. Some of these excitations favor a four-defect state, such as the one which produces the $3\,^1A_g$ state at $U=0$, shown in Fig. 6. In terms of the spin-Peierls picture at high U/t_0, the $2\,^1A_g$ lattice configuration results from a competition between spin excitations involving independent spins, and excitations involving bound triplet coupled pairs as shown in Fig. 8. In the case of well-separated solitons on the long chain, two spin-$\frac{1}{2}$ excitations can be combined to describe a singlet and triplet excitation which are nearly degenerate. However, on short chains, again because of the strong overlap of the defect wave functions, the singlet-triplet splitting is increased and the lowest singlet excitation results from coupling two ^3B_u soliton pairs forming a $2\,^1A_g$ state with four defects. In this case, the excitation energy of the $2\,^1A_g$ state is found at roughly twice that of the ^3B_u state containing two solitons.

In either case the lowest-lying electronic excitations in the model are triplet excitations. These are inaccessible by direct photoexcitation, though they may be populated indirectly after photoexcitation into higher-lying singlet states. The lattice relaxation surrounding the ^3B_u excitation is quite similar in the $N=16$ and $N=64$ cases studied above, namely, the ^3B_u promotes dissociation of a kink-antikink pair. A simple calculation in the $U=0$ limit shows that the resulting kinks are neutral, and indeed our calculations with electron-electron interactions included show that the defects repel and dissociate even in the presence of the Coulomb repulsion term in the Hamiltonian. For the shorter chains, these defects are confined only by the finite system size. An important consequence is that for extended degenerate ground-state polymers, once formed the low-lying triplet excitation will be expected to spontaneously decay into two decoupled spin-$\frac{1}{2}$ centers.

We summarize this situation for the degenerate ground-state systems with the schematic level diagrams of Fig. 19(a). The left-hand panel illustrates the level ordering expected in the noninteracting ($U=0$) limit, and the right-hand panel extends the description to the situation with an on-site repulsion interaction of intermediate strength. The ground state is an even-parity singlet with a homogeneous bond alternation pattern in either case. In the noninteracting limit the lowest-lying excitation is the ^1B_u excitation across the gap (degenerate with the ^3B_u excitation). The singlet decays spontaneously to the spinless charged kink-antikink pair as shown. The triplet (not shown) decays to neutral spin-$\frac{1}{2}$ solitons at the same energy. In the presence of interactions the photoexcited pair may encounter a different fate. One relaxation channel, confined to the ^1B_u surface gain leads to a relaxation to the K^+K^- state as in the $U=0$ case. However, emission of an odd-parity phonon can lead to a crossing to the lower-lying $2\,^1A_g$ surface. For the short systems we found that this state may be approximately represented as a bound quartet of "neutral" kinks, though for longer systems it becomes increasingly difficult to apply this decomposition (there is a relatively smaller admixture of the higher single-particle excitations responsible for two of these neutral excitations, and the state resembles more closely a two-defect state). In our model, there are no perturbations which couple to the spins of the defects; how-

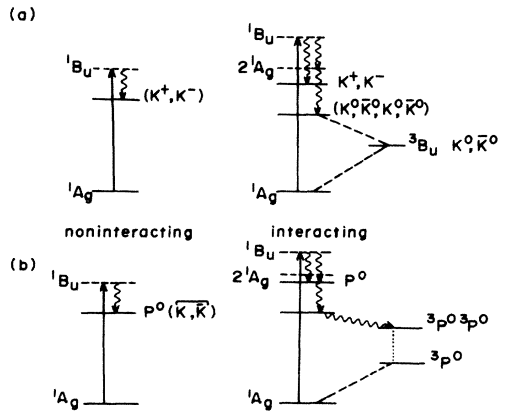

FIG. 19. Schematic level diagram for relaxation and decay of photoexcited states in the noninteracting and interacting cases for (a) degenerate system, (b) nondegenerate system.

ever, in the presence of such perturbations a further relaxation coupling to the triplet manifold is possible. Note, however, that even for our calculations on the 16-site systems, the $2\,^1A_g$ state is interpreted as a *bound* pair of ^3B_u excitations, so that conversion to the triplet manifold would require thermal activation over an energy barrier required to dissociate the pair. Once formed on an extended system the resulting ^3B_u state resides on a repulsive potential which will lead to spontaneous formation of neutral spin-$\frac{1}{2}$ kinks. For finite systems there is a residual confinement of this pair due to the finite system size. Ultimately recombination of two such mobile spin-$\frac{1}{2}$ objects could return the system to the ground state. For the degenerate ground-state polymer, photoexcitation can thus lead to either charged or neutral structural excitations. The charged states occur only on the ^1B_u surface. The neutral excitations are in fact energetically favored and this latter relaxation channel can only be prevented by a very rapid relaxation to the K^+K^- state on the ^1B_u surface, from which the kinetics of the relaxation to the $2\,^1A_g$ surface may be expected to be extremely slow.

The situation is slightly modified for a polymer with a nondegenerate ground state. A schematic level diagram for this case is given in Fig. 19(b). For the model without interactions the lowest-lying singlet excitation again corresponds to promotion of a particle across the Peierls gap. This drives a structural relaxation in which the electron and hole are self-localized in a neutral polaron, with the confinement potential now binding the KK pair. The related triplet excitation is degenerate with this state for $U=0$. When interactions are turned on, the dipole allowed ^1B_u surface leads to a very similar relaxed lattice configuration labeled P^0 in the right-hand panel. Qualitatively new structures are found on the lower-lying $2\,^1A_g$ surface. As in the degenerate ground-state case this surface can be populated only indirectly by radiationless decay from the ^1B_u surface. However, the even-parity singlet relaxes to a structure which can be characterized as a "two-polaron" state in Fig. 18. The interactions between these polarons is *repulsive* (they are confined only by finite system size in Fig. 18), so that this relaxation channel will quickly produce two weakly interacting neutral triplet excitations labeled $^3P^0$ in the figure. These triplets can be interpreted as the states which would be produced in the $U=0$ limit by single-particle excitations across the gap with the unpaired electrons coupled to a spin triplet. The further decay of these triplets to isolated spin-$\frac{1}{2}$ "kinks" is prohibited by the confinement term in the Hamiltonian. Spontaneous decay to the ground state is also forbidden because of the spin of the defect. Thus photoexcitation in conjugated polymers with a nondegenerate ground state in this model yield neutral spin-1 polarons as the long-lived excited states. It is interesting to speculate on the process by which such excitations can ultimately return to the ground state. In the presence of perturbation which couple to the spin of the defect, interconversion to a singlet configuration should be possible; in this case either radiative or radiationless coupling to the ground-state surface should be possible. However, we believe that it is unlikely that the luminescence actually observed in prototypical nondegenerate systems such as cis $(CH)_x$ (Refs. 25 and 26) originates from this low-lying polaron state (the Stokes shift which would accompany emission from this state is much larger than that seen experimentally), but instead from excitations which self-trap in the polaron associated with the ^1B_u surface.

Thus, in addition to the stable photoexcitations predicted in the $U=0$ limit of this model (spin-0 charged kinks for the extended degenerate ground-state system and confined spin-0 polarons in the nondegenerate systems) we find that the presence of an interelectronic repulsive potential leads to a rich spectrum of competing relaxed neutral structures. For the degenerate ground-state polymer, lower-lying singlet excitations, representing bound neutral triplet excitations are obtained. If these are separated to form isolated triplet centers, the products spontaneously decay to form isolated spin-$\frac{1}{2}$ neutral excitations. This relaxation pathway may be inhibited either by finite systems size (an extrinsic mechanism) or by an intrinsic confinement potential such as occurs in conjugated polymers with a nondegenerate ground state. In this latter case for sufficiently strong confinement the low-lying even-parity singlet excitation is unstable to decay into isolated neutral triplet polarons, which persist as the "stable" long-lived excited states.

ACKNOWLEDGMENTS

We are grateful to Dr. J. Orenstein, Dr. S. T. Chui, and Dr. F. D. M. Haldane for a number of helpful discussions. This work was supported under National Science Foundation (NSF) Grant No. DMR-84-05524. E.J.M. also gratefully acknowledges support from the Alfred P. Sloan Foundation.

[1]W. P. Su, J. R. Schrieffer, and A. J. Heeger, Phys. Rev. B **22**, 2099 (1980); **28**, 1138(E) (1983).
[2]H. Takayama, Y. R. Lin-Liu, and K. Maki, Phys. Rev. B **21**, 2388 (1980).
[3]S. Kivelson and D. E. Heim, Phys. Rev. B **26**, 4278 (1982).
[4]J. E. Hirsch, Phys. Rev. Lett. **51**, 296 (1983).
[5]S. Mazumdar and S. N. Dixit, Phys. Rev. Lett. **51**, 292 (1983).
[6]D. Baeriswyl and K. Maki, Phys. Rev. B **31**, 6633 (1985).
[7]G. W. Hayden and E. J. Mele, Phys. Rev. B **32**, 6527 (1985).
[8]J. E. Hirsch and M. Grabowski, Phys. Rev. Lett. **52**, 1713 (1984).
[9]H. Fukutome and M. Sasai, Prog. Theor. Phys. **69**, 1 (1983); **69**, 373 (1983).
[10]Z. G. Soos and S. Ramasesha, Phys. Rev. B **29**, 5410 (1984).
[11]D. K. Campbell, T. A. DeGrand, and S. Mazumdar, Phys. Rev. Lett. **52**, 1717 (1984).
[12]S. Mazumdar and D. Campbell, Phys. Rev. Lett. **55**, 2067 (1985).
[13]B. Hudson and B. Kohler, Synth. Metals **9**, 241 (1984).
[14]K. Schulten, I. Ohmine, and M. Karplus, J. Chem. Phys. **64**, 4422 (1976); P. Tavan and K. Schulten, *ibid.* **70**, 5407 (1979).
[15]M. Grabowski, D. Hone, and J. R. Schrieffer, Phys. Rev. B

31, 7850 (1985).
[16]A. C. Lasaga, R. J. Aerni, and M. Karplus, J. Chem. Phys. **73**, 5230 (1980).
[17]J. W. Bray and S. T. Chui, Phys. Rev. B **19**, 4876 (1979).
[18]J. E. Hirsch, Phys. Rev. B **22**, 5259 (1980).
[19]P. Lowdin, J. Chem. Phys. **19**, 1396 (1951).
[20]S. N. Dixit and S. Mazumdar, Phys. Rev. B **29**, 1824 (1984).
[21]F. D. M. Haldane, Phys. Rev. B **25**, 4925 (1982).
[22]S. A. Brazovskii and N. N. Kirova, Pis'ma Zh. Eksp. Teor. Fiz. **33**, 6 (1981) [JETP Lett. **33**, 4 (1981)].
[23]Y. Onodera, Phys. Rev. **30**, 775 (1984).
[24]B. S. Hudson, B. E. Kohler, and K. Schulten, in *Excited States,* edited by E. C. Lim (Academic, New York, 1982).
[25]L. Lauchlan, S. Etemad, T. C. Chung, A. J. Heeger, and A. G. MacDiarmid, Phys. Rev. B **24**, 1 (1981).
[26]D. B. Fitchen, Synth. Metals **9**, 341 (1984).